Math. Model. Nat. Phenom.
Vol. 6, No. 5, 2011, pp. 157-183
DOI: 10.1051/mmnp/20116508

A Survey on Mathematical Modelling of Deposition in Waxy Crude Oils

A. Fasano[1], **L. Fusi** [1,*], **S. Correra**[2], **M. Margarone**[2]

[1] Dipartimento di Matematica "U.Dini" - Viale Morgagni 67/a -50134 Firenze
[2] eni exploration & production - Via Emilia 1 - 20097 S. Donato Milanese, Milano

Abstract. Waxy Crude Oils (WCO's) are characterized by the presence of heavy paraffins in sufficiently large concentrations. They exhibit quite complex thermodynamical and rheological behaviour and present the peculiar property of giving rise to the formation of segregated wax deposits, when temperature falls down the so called WAT, or Wax Appearance Temperature. In extreme cases, segregated waxes may lead to pipeline occlusion due to deposition on cold walls. In this paper we review the mathematical models formulated to describe: (i) wax cystallization or thawing in cooling/heating cycles; (ii) the mechanisms of mass transport in saturated non-isothermal solutions; (iii) the experimental device used to measure wax solubility and wax diffusivity; (iv) wax deposition in pipelines carrying a warm, wax-saturated WCO through cold regions; (v) wax deposition accompanied by gelification during the cooling of a WCO under a thermal gradient.

Key words: waxy crude oils, molecular diffusion, mathematical models, free boundary problems
AMS subject classification: 80A20, 76R50, 35R35

1. Introduction

Mineral oils are mixtures of many different hydrocarbons including various impurities. If we consider their content in *alkanes* (or *paraffines*), usually classified in terms of the number of carbon atoms in the molecule (e.g. C_nH_{2n} is in the class C_n of n-alkanes) we may define waxy crude oils (WCO) those particularly rich of n-alkanes with $n \geqslant 17$ (see Figure 1).

*Corresponding author. E-mail: fusi@math.unifi.it

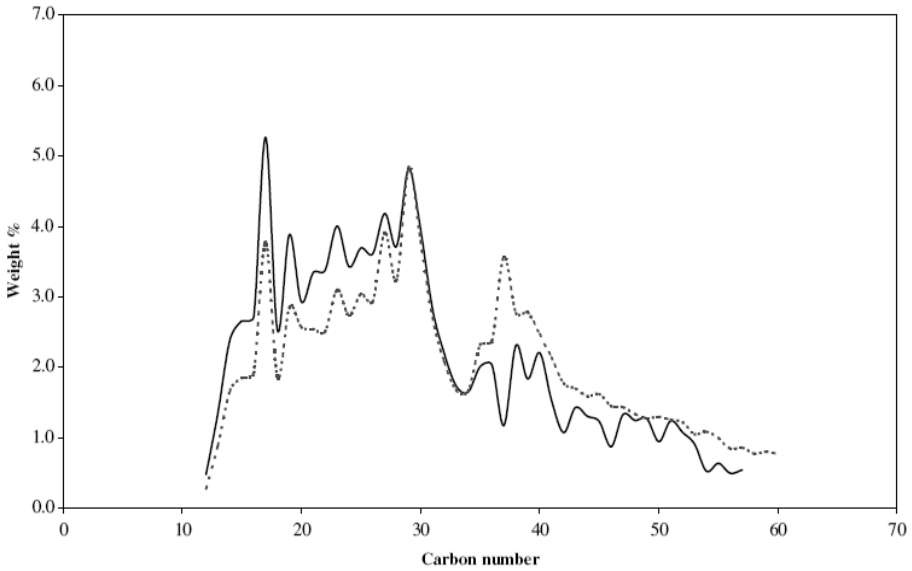

Figure 1: Example of a GC distribution plot of two WCO's

Due to the significant presence of such heavy components and to their heterogeneity, WCO's exhibit very peculiar thermodynamical and rheological properties. Basically, WCOs are characterized by a specific temperature, which is of extreme importance for scientists and engineers handling with these fluids. When the oil is being extracted from reservoir, the temperature may drop below a certain value (the so called Cloud Point or Wax Appearance Temperature, WAT), at which waxes start to solidify and may deposit on the pipe walls (see for example [25]). The most striking consequence can be seen when a WCO is pumped e.g. through a submarine pipeline. If the inlet temperature is e.g. $60 \div 80\ ^o\,C$, the outer temperature being around $4\ ^o\,C$, a radial thermal gradient arises in the pipeline despite thermal insulation, which along a considerable portion of the duct is quite large and mainly confined in a layer close to the pipe wall, since the flow is generally turbulent. As we shall see, such a gradient is able to drive the heavy alkanes to the pipe wall, creating a solid deposit. The deposit can grow to a point that the pipe is eventually occluded. This fact alone explains the importance of predicting the wax deposition rate. This is the main subject we want to treat here. Its tremendous complexity is clearly rooted in the heterogeneity of the material and is further increased by the difficulty of having reliable methods in experiments with WCOs. Moreover, wax deposition can be the result of (and is anyway accompanied by) various concurrent processes, that all need to be modelled.

Various conjectures have been made to provide a theoretical basis to the phenomenon of wax deposition in pipelines in the presence of radial thermal gradients. One mechanism that certainly contributes is molecular diffusion, which will be discussed in some details later. On deposition of waxy gels, a milestone paper is [31], where authors developed a study of the deposition and ageing of wax-oil gel that is formed during the flow of waxy oils in cooled pipes and validated a diffusive model with their own experiments. A concurrent phenomenon that eventually produces a

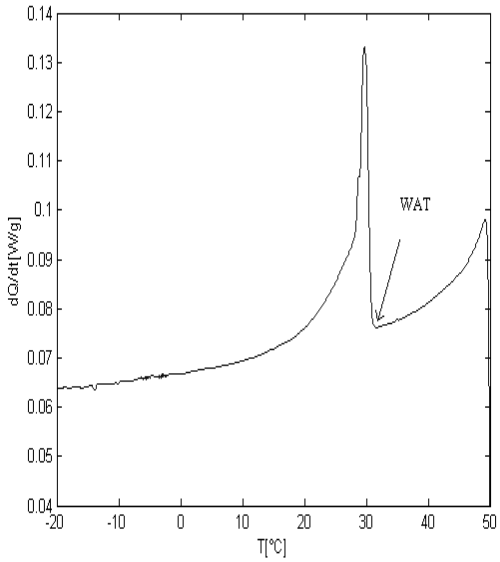

Figure 2: A DSC curve during the cooling of a sample of C36 at 2.5% in decane: the peak indicates the crystallization of wax.

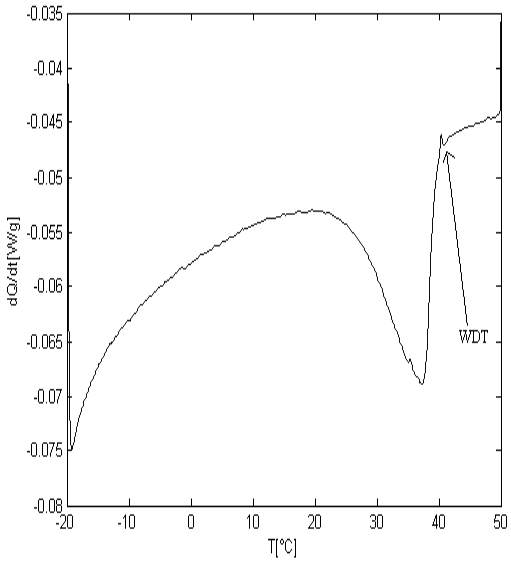

Figure 3: A DSC curve during the heating of a sample of C36 at 2.5% in decane: the peak indicates the dissolution of wax crystals.

solid layer at the wall is the formation of gel. That happens when wax crystals become sufficiently large and numerous to entangle forming a network in which liquid oil is entrapped. The latter phenomenon occurs at sufficiently low temperatures, though above the solidification point of the entire system.

So far we have talked about "wax diffusion", "wax deposition", "wax gelification", but such expressions are definitely misleading, since, as we said, a crude oil is a mixture of many components. Indeed the presence of such components is the source of many difficulties, since the behaviour of a multi-component mixture is far more complicated than, for example, the one of a standard solution (solvent + solute). This is true for what concerns the rheology, the thermodynamics and the diffusive transport, i.e. all the main processes that play a role in the evolution of WCO's. However, in order to formulate mathematically treatable models, a typical simplified scheme of a WCO could be generally adopted in which just two components are considered: the "light" component, acting as the solvent, and the dissolved "wax", considered as a single substance whose properties are obtained by averaging the ones of the various components. In [24] and [15], for example, an idealized two-component system has been reproduced in laboratory, experimenting with solutions of $C36$ in $n-$decane in order to investigate the crystallization process using a DSC, as well as the phenomenon of wax migration under thermal gradients. We will shortly comment the calorimetric results in Section 2.

Still referring to the simplified scheme of the two-component system, in Section 3. we will deal with the process of molecular diffusion in non-isothermal saturated solutions (wax migration and deposition on cold walls), a phenomenon associated to the temperature dependence of wax solubility. The main difficulty is to measure the diffusivity of dissolved wax. A device that is used

to this end and that exploits the phenomenon of wax deposition is the so-called cold finger, which can be static or agitated by impellers. The theoretical basis of such a device has been investigated in [7], [8] and will be described in Section 4.

The application to the wax deposition process in pipelines carrying WCO in turbulent flow will be illustrated in Section 5. The reference paper is [9]. Finally, in Section 6., we will summarize the highly complex problem of gel formation, accompanied by the formation of a solid wax deposit, during the cooling of a static saturated solution [19]. A full description of the flow problem with wax deposition and gelification is still missing.

To our knowledge, the present paper is the first attempt to review mathematical models connected to wax deposition with modelling of lab experiments. On the physical mechanisms involved in wax deposition, apart from one of the first works on this subject [5], a good and critical review can be found in [4] and in [25].

The main source of the material we are going to illustrate comes from a long collaboration with eni exploration and production (and its former R&D company EniTecnologie, San Donato Milanese, Italy), which has involved also I2T3 (Industrial Innovation Through Technological Transfer, Firenze, Italy) and more recently the Donegani Institute (the eni research centre for non conventional energy, Novara, Italy) and the Department of Organic Chemistry "U. Schiff" of University of Florence (Firenze, Italy).

2. Calorimetric experiments on the crystallization kinetics

The phenomenon of wax precipitation requires a good knowledge of the solid-liquid equilibrium mechanism involved and different thermodynamical models have been proposed (see [11]-[14], [21], [22], [27]-[34]). The analysis of this phenomenon cannot be separated from the development of experimental methods capable of quantifying the amount of precipitated wax as a function of temperature.

In this section we summarize very briefly the conclusions illustrated in [15] and presented in [24], based on the experiments performed at the Donegani Institute (the eni research centre for non conventional energy, Novara, Italy) and at the Department of Organic Chemistry "U. Schiff" of the University of Florence (Florence, Italy).

DSC (differential scanning calorimetry) is a well known and reliable technique commonly used to this aim because of its simplicity and capacity to develop routine essays. Important informations on this technique can be found, for instance, in [12]. DSC results have been analyzed in order to formulate a specific kinetics able to predict the amount of precipitated wax under given thermal conditions.

DSC experiments have been performed using $n - C36$ in $n-$decane (Carlo-Erba) at various concentrations. It has been observed that the samples keep memory of the thermal history and therefore they have been kept for sufficiently long time over $90\ ^o\ C$ before starting cooling/heating cycles at constant rate $(1-2\ ^oC/\min)$.One of the aims was to determine the WAT (Wax Appearance Temperature) and the WDT (Wax Disappearance Temperature). The results, as expected, proved that

(i) The diagram of the heat released during cooling (or equivalently the crystallization rate) is very different from the one of the heat absorbed during heating (measuring the thawing rate) (see Figures 2, 3 from [15]). In particular WAT is systematically lower than WDT, the difference depending on the cooling rate, emphasizing the presence of supercooling.

However,

(ii) Experiments performed by rapid cooling to a given temperature showed that the relaxation time to the corresponding asymptotic crystal fraction is rather short (see Figures 4, 5).

This phenomenon is particularly important, since it justifies the assumption (frequently adopted in the sequel) that in a slow cooling process practically no solid segregated phase may survive in an unsaturated solution and that supersaturation phenomena may be neglected. An equation which can describe sufficiently well the crystallization kinetics during cooling is the following

$$\frac{\partial G}{\partial t} = K(c - c_s)_+^q G^p, \tag{2.1}$$

where K, p and q are a positive constant, c is total wax concentration and G is the solid wax concentration. Denoting with $c^* = c + G$ the total amount of wax in the sample the general crystallization kinetics can be rewritten as

$$\frac{\partial G}{\partial t} = K(c^* - G - c_s)_+^q G^p. \tag{2.2}$$

In the above equation the quantities $c_s(T)$ and K are unknown. They can be determined by fitting expression (2.2) with the experimental data obtained through DSC. Depending on whether the system is heated or cooled we will obtain different $c_s(T)$ and K. In what follows we describe the procedure used to obtain the solubility curve when the system is cooled (the solubility curve in the case the system is heated can be determined in an analogous manner).

We consider a sample of our mixture, containing a total wax concentration $c^\star$, in which the temperature decreases from a temperature T_0 to a certain temperature $T_{iso} < T_{WAT}$. After having reached the value $T = T_{iso}$ the temperature remains unchanged:

$$T(t) = \begin{cases} T_0 - \lambda t, & t \in [0, t_{iso}] \\ T_{iso}, & t \in [t_{iso}, t_e]; \end{cases}$$

where $T_{iso} = T_0 - \lambda t_{iso}$, $\lambda > 0$ is the constant cooling rate and t_e is the final time of the experiment. The segregation rate is given by (2.2) where $c_s = c_s(T_{iso})$ and K are unknown. By rearranging the DSC data we are able to obtain the experimental values $\dot{G}_{exp}(t_i)$, at the instants $t_i \in [t_{iso}, t_e]$. Thus, by fitting the curve given by (2.2) to these data, we can estimate the unknown quantities c_s and K.

Given a total wax concentration $c^\star$, this procedure has been performed for different values of T_{iso} and using, in particular, $q = 1$ and $p = 3/4$ (the latter comes from the assumption that the crystals have a spherical shape, see [28] for details). In order to be sure that, given T_{iso}, the value c_s were correct, it has been checked that the procedure gave the same values of c_s, also for

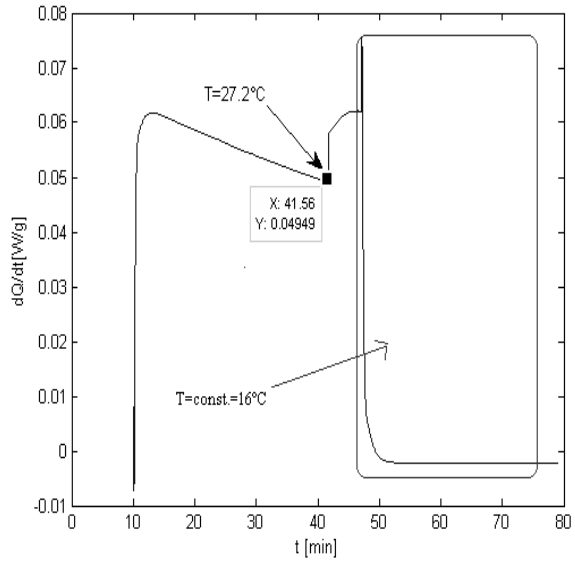

Figure 4: a DSC curve obtained by stopping the temperature at 16^o C during the cooling.

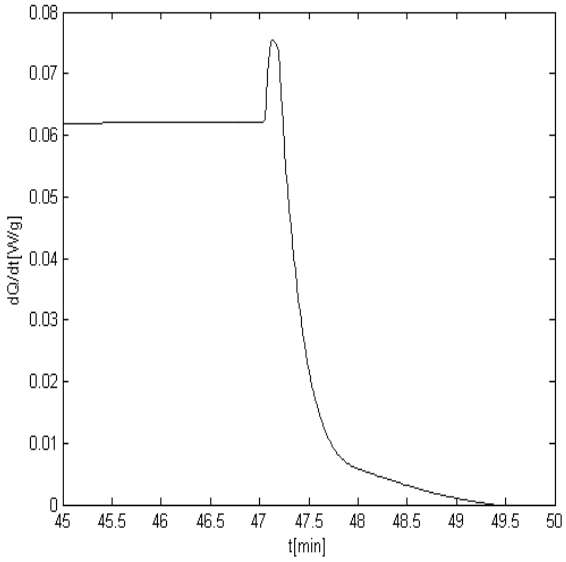

Figure 5: zoom on the framed part of the curve of Fig. 4

mixtures having different total wax concentrations $c^\star$. The result has been satisfactory since the several values of c_s deriving from the different mixtures, are all approximately equal. Finally, the interpolation of the points $(T_{iso}, c_s(T_{iso}))$ (at various T_{iso}) has allowed to construct the solubility curve (as shown in Figure 6). Figure 6 shows a solubility curve obtained by means of the procedure exposed above (cooling the sample). We notice that the solubility curve, $c_s(T)$, is between the two curves which can be ideally drawn by taking the experimental values of WAT and WDT and, particularly, it is more close to the latter.

Kinetics of type (2.1) are inspired to the classical theory of Kolmogorov and Avrami (see [1]-[3] and [23]), developed for solidification processes driven by crystal nucleation and growth, which have generated a large literature. The model proposed in [26] is also in the same spirit.

3. Molecular diffusion in non-isothermal saturated solutions

Suppose now that cooling occurs in a spatially nonuniform way and that supersaturation is not allowed. Since the solubility (concentration at saturation) is an increasing function of temperature, in addition to the phenomenon of crystals segregation, the presence of a thermal gradient in a saturated solution produces a concentration gradient proportional to the thermal gradient, forcing the solute to diffuse. It is easy to realize that if the second derivative of solubility with respect to temperature is positive, then the constraint that the solution cannot be supersaturated requires that more crystals are produced in order to respect mass balance. Thus the evolution of the system is necessarily complicated.

Even if solubility is just a linear function of temperature, the solute migration from warmer to

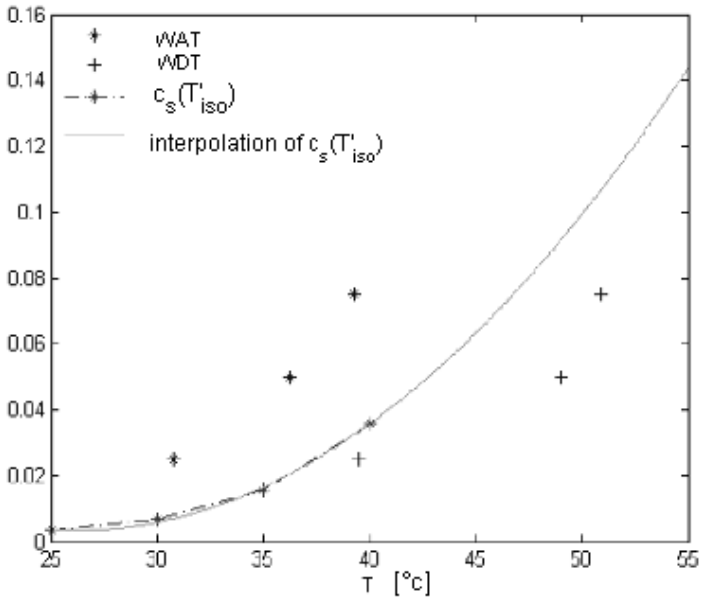

Figure 6: The solubility curve

colder regions has some nontrivial consequences at the boundaries of the system. Take for simplicity a one dimensional geometry, namely a layer $0 < x < L$, with uniform initial concentration c_o and uniform temperature T_o, such that the solution is saturated. It means that if $c_s(T)$ is solubility, then $c_s(T_o) = c_o$. In addition suppose that $c_s'(T) = \beta > 0$ is constant. Now keep the wall $x = L$ at the temperature T_o, while the wall $x = 0$ is cooled down at some given rate $a > 0$: $T(0,t) = T_o - at$. To make the problem even simpler suppose that the thermal diffusivity D_T is much larger than the solute diffusivity D and that the cooling rate is small enough so that the thermal field across the layer can be considered quasi-steady, i.e. linear in x.

Depending on the initial condition (fully saturated, partial saturated or fully unsaturated), the system shows various behaviours presenting free boundaries that separate the regions where the solution is fully or partially saturated. If, for instance, the system is initially fully unsaturated, i.e. $c^* < c_s(T_o)$ then segregation will not occur until some time $\hat{t}$ when $c_s(T_o - a\hat{t}) = c^*$. At time $\hat{t}$ a region $Q^+ = \{0 < x < s(t)\}$ will appear where $G > 0$ and $c(x,t) = c_s(T(x,t))$. In case of thermodynamical equilibrium between the solid and the dissolved phase, for $t > \hat{t}$, the system will

be governed by

$$\begin{cases} \dfrac{\partial G}{\partial t} - D_G \dfrac{\partial^2 G}{\partial x^2} = -\dfrac{\partial}{\partial t} c_s(T(x,t)) + D \dfrac{\partial^2}{\partial x^2} c_s(T(x,t)), & (x,t) \in Q^+, \\ \dfrac{\partial c}{\partial t} - D_G \dfrac{\partial^2 c}{\partial x^2} = 0, & (x,t) \in [0,L]/Q^+. \end{cases} \tag{3.1}$$

The boundary conditions are

$$\left[D_G \frac{\partial G}{\partial x} + D \frac{\partial c_s(T)}{\partial x} \right] \Bigg|_{x=0} = 0, \tag{3.2}$$

$$\left[\frac{\partial c}{\partial x} \right] \Bigg|_{x=L} = 0, \tag{3.3}$$

while the free boundary condition expresses mass balance

$$\left[D_G \frac{\partial G}{\partial x} + D \frac{\partial c_s(T)}{\partial x} - D \frac{\partial c}{\partial x} \right] \Bigg|_{x=s} = 0. \tag{3.4}$$

Another important aspect is the evolution of the deposit layer at the cold wall. As a first step one may neglect the deposit thickness and assume that all the incoming dissolved wax precipitates and sticks to the wall. If, on the other hand, we want to incorporate the growth of a layer of thickness $\sigma(t)$ we can write

$$[\rho - c_s(T(\sigma,t)) - G(\sigma,t)]\, \dot{\sigma} = D \frac{dc_s}{dT} \frac{\partial T(\sigma,t)}{\partial x}. \tag{3.5}$$

as long as in region near the cold wall the solution is saturated by wax. Various models describing different conditions and geometries can be found in papers [6], [16], [17], [18], where analytical results such as existence and uniqueness are proved. In particular in [17] the authors propose a weak formulation for a general 3D domain for which weak solutions have been proved to exist. Subsequently, in [20] a one dimensional problem is formulated in the framework of the model presented in [17] and existence of local classical solutions is proved by means of fixed point techniques.

4. The cold finger device

The so-called cold finger is a device used to determine wax diffusivity and solubility from deposition measures. This apparatus consists in a cylindrical container filled with the oil in which another cylinder (the "cold finger") is co-axially inserted (see Figure 7). The walls of the cylinders are thermally controllable so that the solution can be kept under a prescribed steady thermal gradient. When the solution is saturated by wax, the temperature difference between the warm (outer) wall and the inner (cold) wall induces, in turn, a concentration gradient of dissolved wax which starts to migrate towards the cold finger. As the dissolved wax reaches the cold finger surface it precipitates, forming a layer of deposit that is subsequently collected and weighed. In [7], [8] two mathematical models for the cold finger apparatus have been proposed, distinguishing between two different situations :

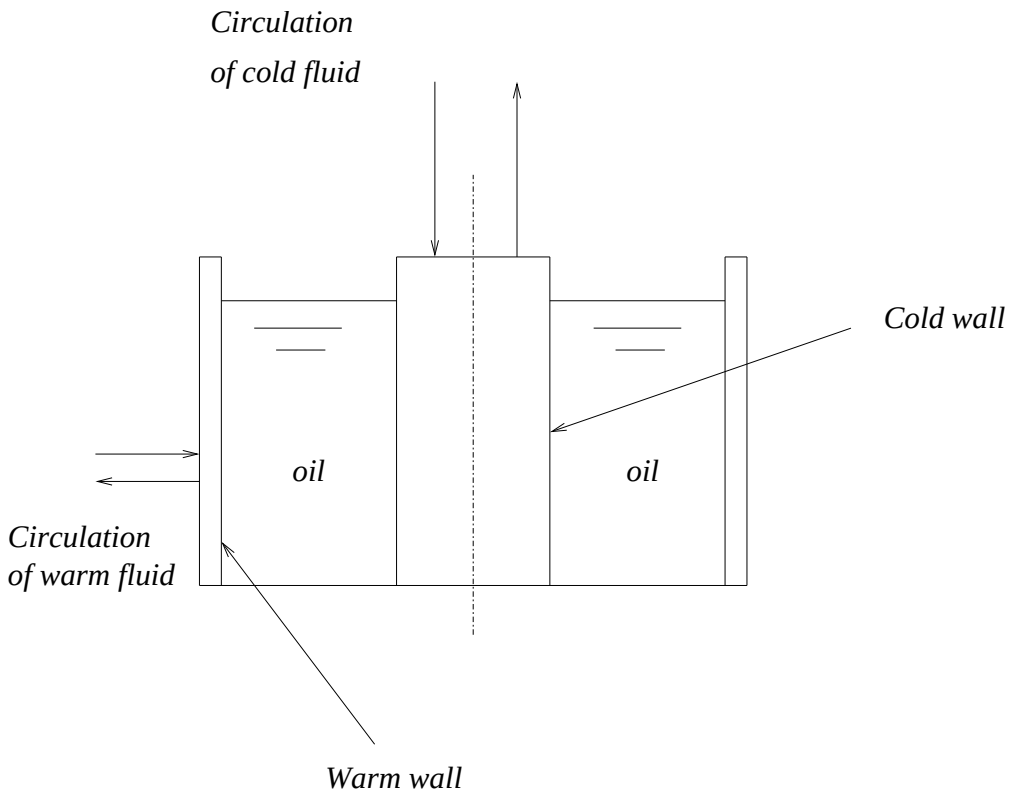

Figure 7: Sketch of the cold finger device.

(i) the oil is immobile

(ii) the solution is stirred.

The models have been developed in cylindrical geometry and assuming that the thermal profile is in its steady state. The main scope is to determine predictive formulas for the wax deposit and to use them for deducing the values of wax solubility c_s and liquid wax diffusivity D. In [7] it has been shown that for typical temperature ranges of cold finger experiments wax solubility can be considered as a linear function of temperature. Therefore we write

$$c_s(T) = c_o + \beta(T - T_o), \tag{4.1}$$

where c_o is the solubility at temperature T_o. In the static device (i.e. when the oil is not stirred), the solubility gradient β can be determined by means of asymptotic mass measures, that is by means of the amount of deposited mass measured at a sufficiently long time when it is observed that deposit growth has finished. In the asymptotic state the wax concentration in the solution will be the saturation concentration at the temperature of the cold finger. Suppose that m_1 and m_2 are two asymptotic mass measures relative to the cold wall temperatures T_1 and T_2, respectively, and suppose that in both cases the solution is initially saturated by wax and the initial concentration is

c_o. Then mass balance implies that

$$m_i = (c_o - c_s(T_i)) \cdot \frac{R_e^2 - R_i^2}{2R_i}, \qquad i = 1, 2, \tag{4.2}$$

where R_e, R_i are the outer wall radius and the cold finger radius respectively and m has to be intended as deposited mass per unit surface of the cold finger. From (4.1) we have

$$m_i = \beta(T_i - T_o) \cdot \frac{R_e^2 - R_i^2}{2R_i}, \qquad i = 1, 2, \tag{4.3}$$

and we can deduce

$$\beta = \frac{m_2 - m_1}{(T_2 - T_1)} \cdot \frac{2R_i}{R_e^2 - R_i^2}. \tag{4.4}$$

For what concerns the diffusivity, the plots of the deposited mass versus time for different experiments show that, as long as the solution is saturated in the vicinity of the cold finger, mass grows linearly with time, i.e. the derivative (see Figure 8)

$$\frac{dm}{dt} = D\beta \frac{dT}{dr}\bigg|_{r=R_i}, \tag{4.5}$$

is constant. It is clear that if we evaluate the slope of the function $m(t)$ during the linear growth regime, the diffusivity coefficient D can be easily obtained from (4.5). It must be kept in mind that normally the deposit grows not as a thick solid layer, but rather as a gel structure with a large inclusion of liquid oil. Therefore it is important to perform suitable corrections to the mass collected over the cold finger to obtain the real content of solid wax (see [7] to see how to quantify this correction).

Once the parameters β and D are determined we are able to describe the evolution of the system which goes through several stages depending on the initial state of the solution (saturated, partially saturated or unsaturated). In particular, assuming that the temperature at the warm wall is lower that the WAT, the solution is initially completely saturated and the system evolves through three stages: (i) complete saturation; (ii) partial saturation; (iii) complete desaturation. Supposing that the system is in thermodynamical equilibrium (in the sense explained in section 2.), the governing equation of segregated wax during stage (i) is given by

$$\frac{\partial G}{\partial t} = D_G \left(\frac{\partial^2 G}{\partial r^2} + \frac{1}{r} \frac{\partial G}{\partial r} \right), \tag{4.6}$$

where D_G is the diffusivity of the solid wax and with boundary conditions

$$\frac{\partial G(R_i, t)}{\partial r} = 0, \qquad D_G \frac{\partial G(R_e, t)}{\partial r} = -D\beta \frac{\partial T(R_e)}{\partial r}. \tag{4.7}$$

A steady flow of dissolved wax takes place during this stage. The second condition in (4.7) says that such a flow is fed by a progressive depletion of the solid phase. Stage (i) ends when $G(R_e, t) =$

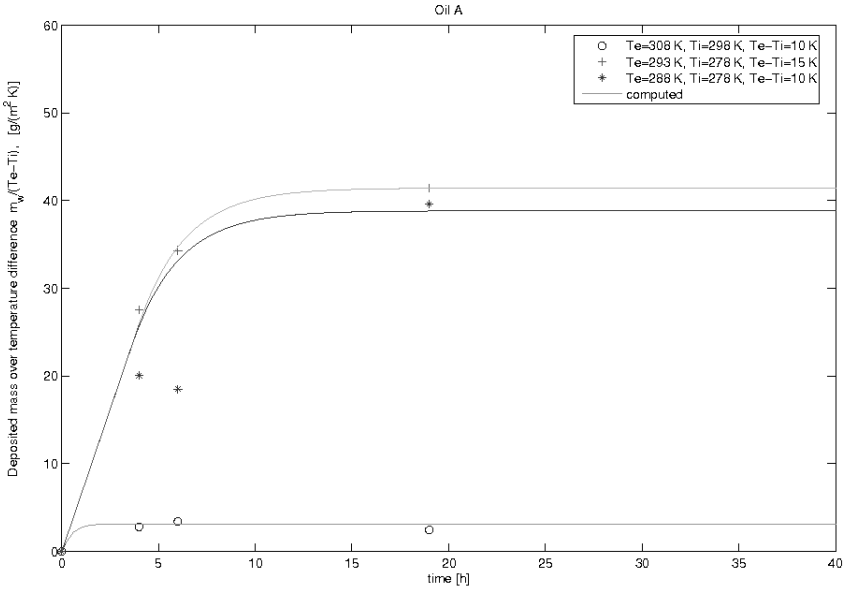

Figure 8: Plot of mass growth in the static cold finger.

0, triggering the appearance of a desaturation front $r = s(t)$ at the warm wall. During stage (ii) equation

$$\frac{\partial G}{\partial t} = D_G \left(\frac{\partial^2 G}{\partial r^2} + \frac{1}{r} \frac{\partial G}{\partial r} \right), \tag{4.8}$$

must be solved in the saturated domain $R_i < r < s(t)$, while in the unsaturated region $s(t) < r < R_e$ the dissolved wax concentration obeys

$$\frac{\partial c}{\partial t} = D \left(\frac{\partial^2 c}{\partial r^2} + \frac{1}{r} \frac{\partial c}{\partial r} \right). \tag{4.9}$$

The boundary conditions are

$$\frac{\partial G(R_i,t)}{\partial x} = 0, \qquad \frac{\partial c(R_e,t)}{\partial r} = 0, \quad G(s,t) = 0, \qquad D_G \frac{\partial G(s,t)}{\partial r} = -D\beta \frac{\partial T(s)}{\partial r} + D \frac{\partial c(s,t)}{\partial r}, \tag{4.10}$$

the latter expressing mass balance at the desaturation front. Stage (ii) finishes when $s(t) = 0$. Then the system enters stage (iii), where we are left with the only equation

$$\frac{\partial c}{\partial t} = D \left(\frac{\partial^2 c}{\partial r^2} + \frac{1}{r} \frac{\partial c}{\partial r} \right), \tag{4.11}$$

with

$$c(R_i,t) = c_s(T_(R_i)), \qquad \frac{\partial c(R_i,t)}{\partial r} = 0, \qquad R_i < r < R_e. \tag{4.12}$$

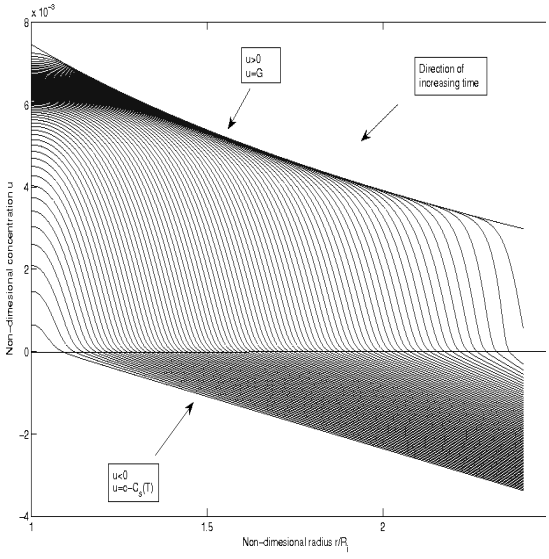

Figure 9: Plot of the function $u = c - c_s$ during stages (i) and (ii).

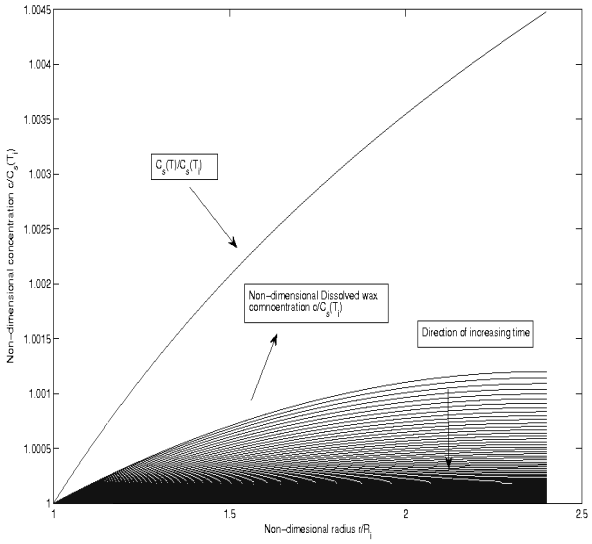

Figure 10: Plot of the function c during stage (iii).

Figures 9, 10 show the behaviour of the system during the three stages. In particular in Figure 9 the plot represents the function

$$u(x,t) = \begin{cases} G(x,t), & r < s(t), \\ \\ c(x,t) - c_s(T(x)), & r > s(t), \end{cases} \tag{4.13}$$

where $r = s(t)$ is the level set $u(s,t) = 0$. Figure 10 represents the evolution of the liquid concentration c during stage (iii).

The static cold finger has one main drawback. The thermal gradient between the cylinders has to be small enough to prevent thermal convection (which modifies the thermal profile in a substantial way). Thus experiments have to use samples of relatively small mass, thus increasing relative errors. A better experimental condition is produced in the presence of stirring. Indeed, in that dynamical condition the main quantities involved can be considered space independent except in two boundary layers near the walls. This circumstance has also the effect of producing larger thermal gradients in the boundary layers, enhancing wax migration. The thickness of the boundary layers are determined writing the heat flux balance at the surfaces separating the homogeneous bulk and the boundary layers. In particular (see Figure 11)

$$r_i = R_i \exp\left\{\frac{k}{hR_i}\right\}, \qquad r_e = R_e \exp\left\{-\frac{k}{hR_e}\right\}, \tag{4.14}$$

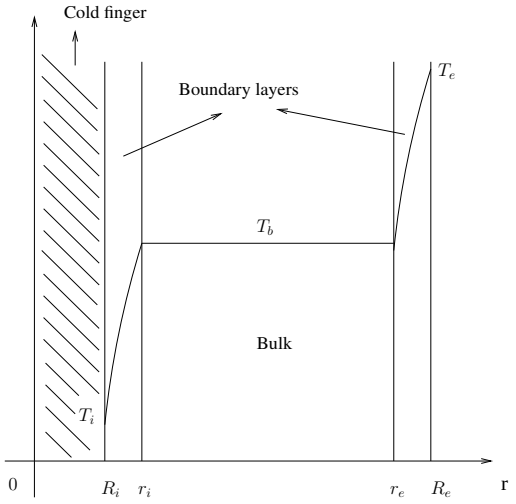

Figure 11: Geometry of the stirred col finger and thermal profile.

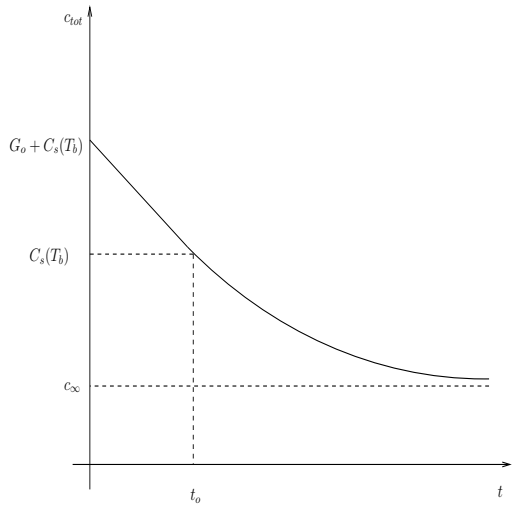

Figure 12: Total wax concentration profile.

where h is the heat transfer coefficient and k is thermal conductivity. The thermal profile is given by

$$\begin{cases} T = T_i + \dfrac{hR_iR_e}{k}\dfrac{(T_e - T_i)}{(R_e + R_i)} \ln\left(\dfrac{r}{R_i}\right), & R_i \le r \le r_i, \\ T_b = \dfrac{R_eT_e + R_iT_i}{R_e + R_i}, & r_i \le r \le r_e, \\ T = T_e + \dfrac{hR_iR_e}{k}\dfrac{(T_e - T_i)}{(R_e + R_i)} \ln\left(\dfrac{r}{R_e}\right), & r_e \le r \le R_e. \end{cases} \tag{4.15}$$

The bulk temperature is obtained imposing that the incoming flux at $r = R_e$ is equal to the outgoing heat flux at $r = R_i$. The mass growth rate per unit surface at the cold wall is given by

$$\frac{dm}{dt} = D\beta \left.\frac{dT}{dr}\right|_{r=R_i} = D\beta \frac{hR_e}{k}\frac{(T_e - T_i)}{R_e + R_i}, \tag{4.16}$$

where the thermal gradient is obtained from $(4.15)_1$. The evolution of the solid phase fraction G is obtained imposing that the rate at which the segregated phase is dissolved equals the deposition rate, i.e.

$$\pi\dot{G}(R_e^2 - R_i^2) = -2\pi R_i D\beta \frac{hR_e}{k}\frac{(T_e - T_i)}{R_e + R_i}. \tag{4.17}$$

The above equation can be integrated providing the function

$$G(t) = G_o - \frac{2DbhR_iR_e}{k}\frac{(T_e - T_i)t}{(R_e + R_i)(R_e^2 - R_i^2)} \tag{4.18}$$

where $G_o = c_o - c_s(T_b)$. Setting $G(t) = 0$ we obtain the desaturation time t_o. Once the bulk is depleted of solid wax, the mass loss due to deposition causes desaturation of the solution up

to the asymptotic limit $c_\infty = c_s(T_i)$. During this stage it may be supposed that the mass growth rate is proportional to the deviation of wax concentration from its asymptotic limit (of course other kinetics may be proposed), i.e.

$$\frac{dm}{dt} = \lambda(c - c_\infty), \tag{4.19}$$

so that mass balance is expressed by

$$\dot{c}\pi(R_e^2 - R_i^2) = -2\pi R_i \lambda(c - c_\infty). \tag{4.20}$$

Integration of the above with the initial datum $c(t_o) = c_s(T_b)$ yields

$$c(t) = c_\infty + (c_s(T_b) - c_\infty) \exp\left\{-\frac{2\lambda R_i}{(R_e^2 - R_i^2)}(t - t_o)\right\}, \tag{4.21}$$

The total wax concentration

$$c_{tot}(t) = \begin{cases} G(t) + c_s(T_b), & 0 \le t \le t_o \\ \\ c(t), & t \ge t_o \end{cases}. \tag{4.22}$$

can then be plotted (see Figure 12). From (4.16) and (4.19) we see that mass growth is initially linear in time t (up to time t_o) and then tends exponentially to its asymptotic value. More precisely

$$m(t) = \lambda(c_s(T_b) - c_\infty)t, \qquad 0 \leqslant t \leqslant t_o \tag{4.23}$$

$$m(t) = m(t_o) + \frac{(R_e^2 - R_i^2)(c_s(T_b) - c_\infty)}{2R_i}\left[1 - \exp\left(-\frac{2\lambda R_i(t - t_o)}{R_e^2 - R_i^2}\right)\right], \qquad t > t_o \tag{4.24}$$

with

$$m(t_o) = \frac{[c_o - c_s(T_b)](R_e^2 - R_i^2)}{2R_i}. \tag{4.25}$$

Figures 13, 14 show the comparison of the evaluated mass deposit growth with experimental data. The two plots are relative to two different temperature differences $\Delta T = T_b - T_i$.

5. Turbulent flow in pipelines crossing cold regions

As observed in the introduction, the problem of wax deposition in non-isothermal pipelining of WCO's is of crucial importance for oil industry. In [9] a model for this phenomenon has been proposed, assuming the normal condition of turbulent flow regime. The only driving mechanism for deposition was supposed to be Fickian diffusion and other concurrent phenomena such as deposit ablation, desaturation, ageing and the possible desaturation of the fluid have been taken into account. Ablation is due to the mechanical action of the flow, while ageing consists in a progressive thickening of the deposit due to the gradual release of the fluid component.

The model describes the flow of a WCO in a pipeline of radius R, assuming that the temperature at the inlet is greater than WAT and that the temperature of the surroundings is lower than WAT.

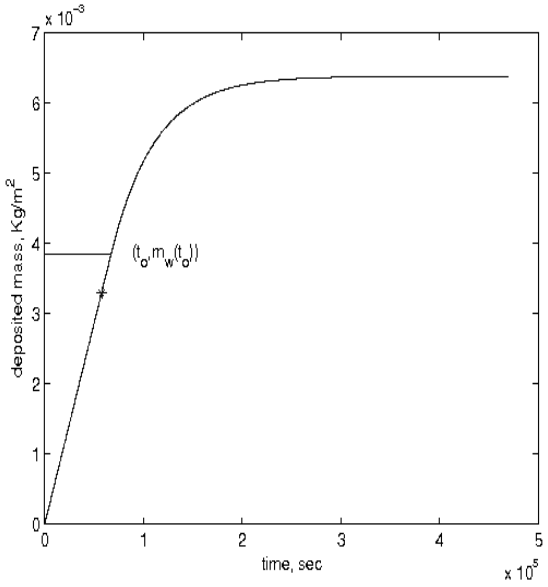

Figure 13: Computed mass growth and experimental data: $\Delta T = 4.4\ ^oK$

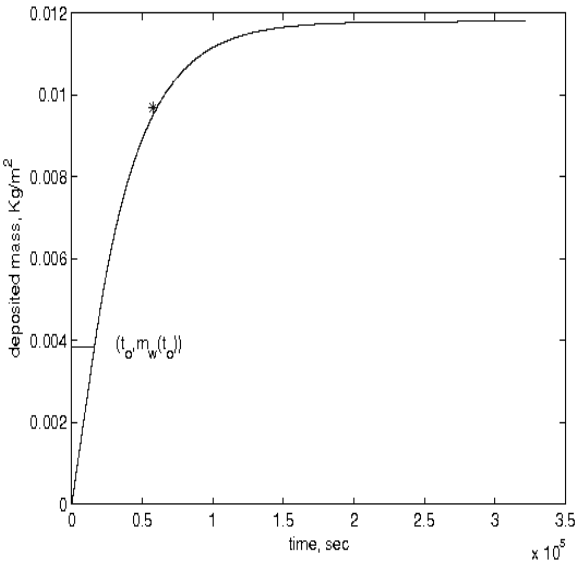

Figure 14: Computed mass growth and experimental data: $\Delta T = 13.8\ ^oK$

The thermal and velocity fields are flat in the turbulent core and can be determined writing the energy and momentum balance. The boundary layers are placed between the solid deposit and the turbulent core, the momentum boundary layer being thicker than the thermal boundary layer. A sketch of the domain is depicted in Figure 15. The diffusive mechanism responsible for deposition occurs in the thermal boundary layer, i.e. the region where there exists a radial thermal gradient. Denoting with $\nu(z,t)$ the radius of the pipeline lumen (progressively reduced by the deposit), the thickness of the thermal boundary layer σ_T is given by

$$\sigma_T = \epsilon_T \nu(z,t), \qquad \epsilon_T = 0.41 \cdot \frac{2\eta Q}{\Delta P \pi \nu^4}, \tag{5.1}$$

where Q is the imposed volumetric flow rate, ΔP is the pressure gradient and η is the viscosity of the fluid (see section 3 of [9] for a full explanation of (5.1)). The temperature profile in the thermal boundary layer is obtained assuming that the heat leaving from the bulk is equal to the one leaving from the wall and that deposition does not alter the thermal properties of the fluid. We suppose that in the thermal boundary layer the thermal profile has the form

$$T(r,z,t) = -a(z,t) R_T(z,t) \ln\left(\frac{r}{R_T(z,t)}\right) + T_c(z,t) \tag{5.2}$$

where $R_T(z,t)$ (deducible from (5.1) is the radius of the region where temperature is independent of r, $T_c(z,t)$ is the bulk temperature and $a(z,t)$ is a coefficient to be determined. We impose a linear heat loss condition at the wall

$$-k\frac{\partial T}{\partial r}(R,z,t) = \frac{k a(z,t) R_T(z,t)}{R} = h\left[T_w(z,t) - T_e(z,t)\right], \tag{5.3}$$

where k is the thermal conductivity of both the fluid and of the deposit, h is the heat transfer coefficient and T_e is the temperature of the surroundings. Then we write the temperature at the wall

$$T_w(z,t) = T(R,z,t) = -a(z,t)R_T(z,t). \tag{5.4}$$

Combining (5.3) and (5.4) we get

$$a(z,t) = \left(\frac{1}{R_T}\right) \frac{1}{\left[\frac{k}{hR} + \ln\left(\frac{R}{R_T}\right)\right]} \left[T_c - T_e\right]. \tag{5.5}$$

so that

$$T(r,z,t) = -\left(\frac{1}{R_T}\right) \frac{1}{\left[\frac{k}{hR} + \ln\left(\frac{R}{R_T}\right)\right]} [T_c - T_e] R_T \ln\left(\frac{r}{R_T}\right) + T_c. \tag{5.6}$$

The temperature of the bulk is determined writing thermal balance for a unit length portion of the turbulent core, which yields (see section 4,5 of [9] for all the mathematical details)

$$T_c(z,t) = [T_o - T_e] \exp\left\{-\int_0^z B(\xi,t)d\xi\right\} + T_e, \tag{5.7}$$

where T_o is the inlet temperature and where

$$B(z,t) = \frac{2\pi\alpha}{Q(1-\epsilon_T)^2\left[\mu + \ln\left(\frac{R}{R_T(z,t)}\right)\right]} > 0. \tag{5.8}$$

We recall that $R_T(z,t)$ is expressed in terms of $\nu(z,t)$, which is still unknown. If we assume that the thickness of each boundary layer is small compared to the turbulent core radius and that the temperatures T_o, T_e are constant, the bulk temperature $T_c(r,z)$ can be considered independent of time and given by

$$T_c(z,t) = (T_o - T_e) \exp\left\{-\frac{2\pi\alpha}{\mu Q} z\right\} + T_e. \tag{5.9}$$

where

$$\alpha = \frac{k}{\rho c}, \qquad \mu = \frac{k}{hR}, \tag{5.10}$$

ρ, c being the density and the specific heat respectively. In this case the temperature in the thermal boundary layer is given by

$$T(r,z) = (T_o - T_e) \exp\left\{-\frac{2\pi\alpha}{\mu Q} z\right\} \cdot \left\{1 - \frac{1}{\mu}\ln\left(\frac{r}{R}\right)\right\} + T_e. \tag{5.11}$$

Deposition is modelled taking into account two opposite mechanisms: molecular diffusion and ablation. The former is responsible for mass transport of dissolved wax towards the pipe walls, while the latter consists in the removal of solid wax, stripped from the deposit because of the drag force exerted by the flux. As a first step it has been assumed that the turbulent core is always

saturated by wax so that wax crystals are present, forming a reservoir which is used to compensate the mass progressively lost because of deposition. Moreover it has been taken into account that the the solid deposit is a mixture formed by wax and liquid oil, introducing the solid wax fraction ψ which may vary due to ageing (the gradual release of the oil entrapped in the deposit). Diffusion has been modelled through Fick's law

$$\vec{j}_{dep} = -\frac{1}{\psi} D\beta \nabla T, \tag{5.12}$$

while ablation rate assuming that the removal rate is proportional to the shear stress τ at the pipe wall, as expressed by

$$j_{abl} = -\frac{A\tau}{\psi} = -\frac{A\eta V}{\psi \varepsilon_m \nu} = -\frac{A\eta Q}{\pi \psi \varepsilon_m \nu^3}, \tag{5.13}$$

where A is an experimental constant and V is the uniform velocity of the turbulent core. The ageing process has been modelled supposing that the growth rate of the solid fraction is proportional to the amount of entrapped liquid, i.e.

$$\frac{\partial \psi}{\partial t} = \frac{1}{t_a}(1-\psi), \tag{5.14}$$

t_a being a characteristic consolidation time.

The evolution of the deposit front ν is obtained writing the mass balance in a unit length portion of the pipeline (see [9] for all the mathematical details), which yields

$$\begin{aligned} \nu^2 = R^2 - \frac{R^2}{T_{WAT}} \left[\frac{(T_o - T_e)}{\mu} \exp\left\{ -\frac{2\pi\alpha}{\mu Q} z \right\} - \frac{A\eta Q}{\pi \varepsilon_m D\beta R^2} \right]_+ \cdot \\ \cdot \frac{2t_a \psi_o}{t_o} \ln\left\{ \frac{1}{\psi_o} \left[\exp\left(\frac{t}{t_a} \right) - 1 \right] + 1 \right\} \cdot H(T_{WAT} - T_w), \end{aligned} \tag{5.15}$$

where t_o is a characteristic deposition time, ψ_o is the initial solid fraction in the deposit and H is the Heaviside function

$$H(z) = \begin{cases} 1 & z > 0 \\ \\ 0 & z \leqslant 0 \end{cases} \tag{5.16}$$

which has been added to ensure that deposition starts only when the wall temperature has dropped below T_{WAT}. The model indeed provides the longitudinal length z_f before which no deposition occurs (this point is obtained imposing that the temperature at the wall equals T_{WAT})

$$z_f = \frac{\mu Q}{2\pi\alpha} \ln\left[\frac{T_o - T_e}{T_{WAT} - T_e} \right] > 0, \tag{5.17}$$

and the longitudinal length beyond which deposition ceases (which may happen if ablation becomes stronger than diffusion)

$$z_e = \frac{\mu Q}{2\pi\alpha} \ln\left(\frac{(T_o - T_e)\pi \varepsilon_m D\beta R^2}{\mu A \eta Q} \right) \tag{5.18}$$

Then one can distinguish three cases

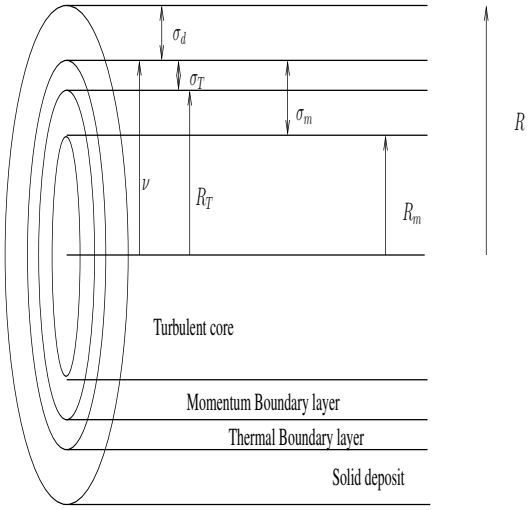

Figure 15: Geometry of the system.

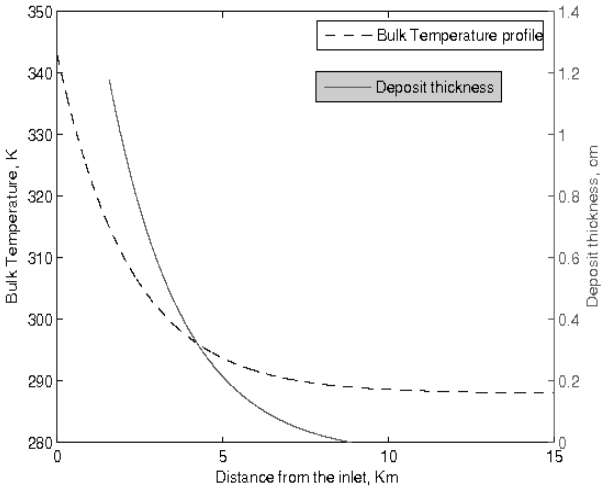

Figure 16: A numerical simulation for the bulk temperature and deposit profiles.

(1.) $z_e > L$. Deposition takes place in the segment $[z_f, L]$.

(2.) $z_f < z_e < L$. Deposition takes place in the segment $[z_f, z_e]$.

(3.) $z_e < z_f$. Deposition never starts.

where L is the length of the pipeline. The last phenomenon that has been taken into account is desaturation. Depending on the initial wax content, on the pipeline length and on the thermal difference between the oil and the surroundings, it may happen that the solid phase suspended in the oil is depleted and the oil becomes unsaturated. The distance z_{des} at which the segregated phase disappears is evaluated imposing that the dissolution rate is equal to the net wax deposition rate, namely

$$\left\{\frac{\partial G}{\partial t} + V\frac{\partial G}{\partial z}\right\}\pi\nu^2 = 2\pi\nu\left\{D\beta\frac{\partial T}{\partial r} - D\beta\frac{\partial T}{\partial z}\frac{\partial \nu}{\partial z} + \frac{A\eta Q}{\pi\varepsilon_m\nu^3}\right\}, \tag{5.19}$$

and writing the steady state solution

$$\hat{G}(z) = G_o + \left[\frac{2A\eta}{\varepsilon_m R^2}(z - z_f) + \frac{D\beta(T_o - T_e)}{\alpha}\left(\exp\{-\frac{2\pi\alpha z}{\mu Q}\} - \exp\{-\frac{2\pi\alpha z_f}{\mu Q}\}\right)\right], \tag{5.20}$$

where $G_o = G(z_f)$. The longitudinal distance z_{des} is found setting $\hat{G}(z) = 0$. Of course the interesting case is when $z_{des} < z_e$. An example of a numerical simulation with the plot of the bulk temperature and deposition profiles is shown in Figure 16. The results obtained in [9] are in reasonable agreement with the data collected in real plants (such data are obtained by weighing the whole mass scraped along the pipe by a suitable device - the so-called pig - and therefore are largely approximated).

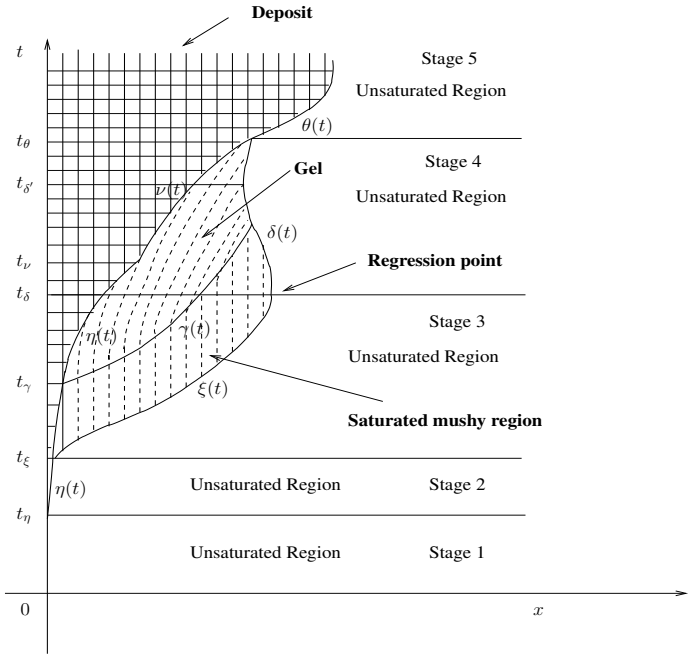

Figure 17: Sketch of the regions and of the interfaces of the various stages.

6. Gelification

In the previous sections we have systematically disregarded the phenomenon of gelification, assuming that the temperature is not in a range at which it takes place in a massive way. Gelification consists in the formation of a network of crystals which, even occupying a very modest volume fraction, can effectively entrap the oil and at the same time reduce the diffusivity of dissolved wax. We will confine ourselves to modelling the process in static conditions.

In order to describe a cooling process with gelification we may start with an isothermal non-saturated solution. In a one-dimensional setting, let the solution occupy the layer $0 < x < L$. At time $t = 0$ wax concentration and temperature have the respective values c^*, T_w , and we are assuming that $T_w > T^*_{cp}$ (namely the WAT corresponding to the concentration c^*). In the process we want to study the temperature at the wall $x = L$ is kept at the value T_w, while the wall $x = 0$ is cooled down to an asymptotic temperature T_a, sufficiently low to produce gelification (namely below the gelification temperature T_{gel}, which is a function of the solid wax concentration G).

In what follows it is important to distinguish between the gel (a semi-solid, still evolving structure) and the deposit, by which we mean a region in which the solid wax content is large enough to prevent the diffusion of the wax dissolved in the residual fluid component. In this section we briefly summarize the long analysis performed in [19]. The corresponding evolution of the system will be considerably complicated and can go through the following stages (see Figure 17 for the mathematical domains corresponding to the various stages):

1. *pre-cooling*: no mass flux, with $T > T^*_{cp}$ everywhere and constant concentration c^*;

2. *onset of deposition at the cold wall*: a small non-diffusive region (deposit) starts growing, while the rest of the layer remains unsaturated. The interface concentration is less than c^*, causing a mass flux that creates the deposit. This stage can be considered as a "waiting time" during which a sufficiently intense wax flux is built up;

3. *onset of saturation*: mass flux in the unsaturated region has become sufficiently large to allow the formation of a saturated region, placed between the unsaturated region and the deposit. This new region will eventually evolve into a gel, which, in turn, undergoes further changes becoming a deposit;

4. *onset of crystal depletion*: in a finite time, the unsaturated phase stops shrinking and expands back, consuming the suspended solid phase;

5. *asymptotic stage*: after the crystal depletion front meets the deposition front, we are back to the situation of stage (ii) and the system goes to its asymptotic state, with a uniform concentration in the unsaturated solution and a deposit, but with no gelified region.

Assuming that the solid phase can exist only in the presence of saturation, the oil entrapped in the gel is necessarily saturated. When the solid crystals concentration is greater than some $G_{gel}(T)$, then gelification occurs. The inverse of $G_{gel}(T)$ is $T_{gel}(G)$ and it is called the gelification temperature. Liquid wax diffusivity is then a function of G which decreases to zero as G ranges from G_{gel} to some $G_{dep} > G_{gel}(T)$. The total wax concentration is defined as

$$c_{tot}(x,t) = G(x,t) + c(x,t), \tag{6.1}$$

with

$$G(x,t) = [c_{tot}(x,t) - c_s(T(x,t))]_+, \tag{6.2}$$

The phase diagram in the (c,T) plane that describes the states crossed during a cooling process is the one depicted in Figure 18, where T_s stands for the oil solidification temperature. The thermal field evolves according to the following system

$$\begin{cases} \dfrac{\partial T}{\partial t} = \left(\dfrac{k}{\rho c_T}\right)\dfrac{\partial^2 T}{\partial x^2}, & 0 < x < L, \quad t > 0, \\ T(0,t) = T_c(t), & t > 0, \\ T(L,t) = T_w, & t > 0, \\ T(x,0) = T_w, & 0 < x < L. \end{cases} \tag{6.3}$$

where ρ is density and c_T is the specific heat and T_c is a smooth function such that

$$T_c(0) = T_w, \qquad \dot{T}_c(t) < 0, \qquad T_s < \lim_{t\to\infty} T_c(t) = T_a < T_{WAT}. \tag{6.4}$$

In [19] it has been proved that the effects due to latent heat of fusion of wax can be safely neglected. In principle the formation of the phase G should generate a sink term in equation $(6.3)_1$.

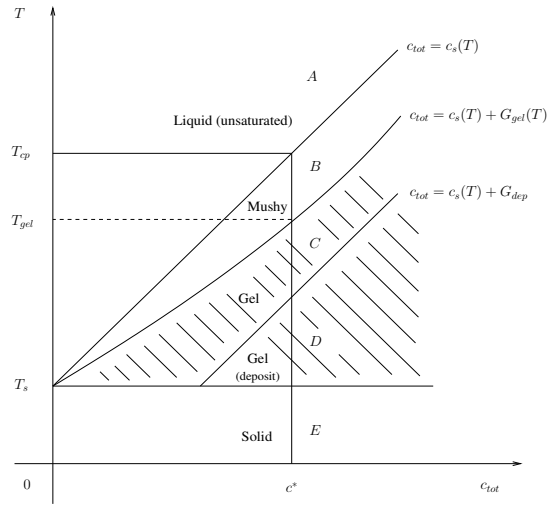

Figure 18: Wax phase diagram.

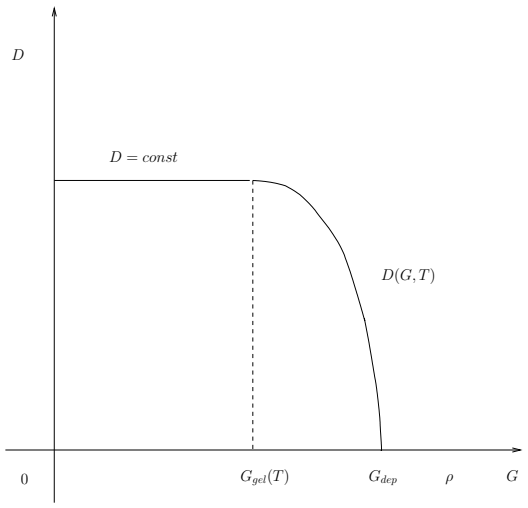

Figure 19: Plot of the diffusivity coefficient at fixed temperature

The possibility of neglecting such a term is fundamental in our approach, since it decouples the evolution of T from the one of G.

A crucial parameter playing a key role in the wax transport is dissolved wax diffusivity D, which is defined as follows (see Figure 19)

$$\begin{cases} D(G,T) = const > 0, & \text{when} \quad G < G_{gel}(T), \\ \dfrac{\partial D(G,T)}{\partial T} > 0, \quad \dfrac{\partial^2 D(G,T)}{\partial T^2} < 0, & \text{when} \quad G_{gel}(T) < G < G_{dep}, \\ \dfrac{\partial D(G,T)}{\partial G} < 0, \quad \dfrac{\partial^2 D(G,T)}{\partial G^2} < 0, & \text{when} \quad G_{gel}(T) < G < G_{dep}, \\ D(G,T) = 0 & \text{when} \quad G > G_{gel}(T), \end{cases} \tag{6.5}$$

(an explicit example of a function satisfying (6.5) is presented in [19]). Stage one is characterized by the fact that $c^* = c_s(T^*_{cp}) < c_s(T_w)$ with no mass transport taking place and with $G = 0$ everywhere in the solution. When the temperature at the cold wall drops below T^*_{cp} (at time t_η) the system enters stage 2. In this phase a deposit region with thickness $x = \eta(t)$ appears at $x = 0$ with $G(\eta, t) = G_{dep}$. The reason why the deposit is formed directly (with no intermediate evolution) is that at this stage the incoming wax flow is too low to feed diffusion in an "immature" deposit. Depending on the cooling rate it may happen that wax flux increases to a point that for some time $t_\xi > t_\eta$ we have

$$D\frac{\partial c}{\partial x}_{|(\eta(t_\xi),t_\xi)} = D\frac{\partial c_s}{\partial x}_{|(\eta(t_\xi),t_\xi)} = D\beta\frac{\partial T}{\partial x}_{|(\eta(t_\xi),t_\xi)}. \tag{6.6}$$

In this situation a *mushy region* $\eta(t) < x < \xi(t)$ starting from $x = \eta(t_\xi)$ appears, leading to stage 3, and characterized by the simultaneous presence of a saturated solution ($c = c_s(T)$) and of a solid

segregated phase ($G > 0$). The curve $x = \xi(t)$ can be called the saturation front. The duration of stage 2 is called the *waiting time* and can be finite or infinite. When the system enters stage 3 the liquid wax concentration $c(x,t)$ satisfies the following problem in the unsaturated phase

$$\begin{cases} \dfrac{\partial c}{\partial t} = \dfrac{\partial}{\partial x}\left(D\dfrac{\partial c}{\partial x}\right), \quad \text{in } \ \xi(t) < x < L, \ \ t > t_\xi, \\ c(x,t_\xi) = \bar{c}(x), \qquad 0 = \xi(t_\xi) \le x \le L, \\ \dfrac{\partial c}{\partial x}(L,t) = 0, \quad t > t_\xi, \\ c(\xi,t) = c_s(T(\xi,t)), \qquad t > t_\xi, \\ \dfrac{\partial c}{\partial x}(\xi,t) = \beta\dfrac{\partial T}{\partial x}(\xi,t), \qquad t > t_\xi, \\ \xi(t_\xi) = \eta(t_\xi), \end{cases} \tag{6.7}$$

where the initial datum $\bar{c}(x)$ is obtained from stage 2. From the mathematical point of view, problem (6.7) can be classified as a free boundary problem with Cauchy data on the free boundary. The related mathematical aspects are discussed in detail in [19]. In the saturated domain $\eta(t) < x < \xi(t)$ $c = c_s(T)$. At this stage the evolution of G is obtained assuming local thermodynamical equilibrium (i.e. assuming that the transition $c_s \to G$ is instantaneous) which yields

$$\left(\frac{\partial}{\partial t} - D\frac{\partial^2}{\partial x^2}\right) c_s(T) = \beta\left(1 - \frac{D}{D_T}\right)\frac{\partial T}{\partial t} = -\frac{\partial G}{\partial t} \tag{6.8}$$

In this model the diffusivity of the solid phase is completely neglected. Integration of the equation above between $t = \xi^{-1}(x)$ (the region where $G = 0$) and t gives

$$G(x,t) = -\mu\left[T(x,t) - T(x,\xi^{-1}(x))\right], \tag{6.9}$$

Note that the presence of the time $\xi^{-1}(x)$ links G to the evolution of the saturation front. The deposit now grows according to

$$[G_{dep} - G(\eta^+,t)]\dot{\eta} = D\beta\frac{\partial T}{\partial x}(\eta,t), \tag{6.10}$$

where $G(\eta^+,t)$ is evaluated by means of (6.9). When, at some time $t_\delta > t_\xi$, the liquid wax diffusing through $x = \xi(t)$ is no longer sufficient to compensate the wax leaving the saturated phase, then the saturation front comes to a stop, i.e. $\dot{\xi} = 0$. From that time on the front reverts its motion and solid crystals are dissolved in order to balance the mass flux on the boundary $x = \xi(t)$ not fully provided by the flux coming from the unsaturated region. At this stage the front $x = \xi$ is renamed with $x = \delta$ (the *depletion* front) which is now moving towards the cold wall. The problem in the unsaturated region becomes

$$\begin{cases} \dfrac{\partial c}{\partial t} = \dfrac{\partial}{\partial x}\left(D\dfrac{\partial c}{\partial x}\right), \quad \text{in } \ \delta(t) < x < L, \ \ t > t_\delta, \\ c(x,t_\delta) = \bar{\bar{c}}(x), \qquad \delta(t_\delta) \le x \le L, \\ \\ \dfrac{\partial c}{\partial x}(L,t) = 0, \quad t > t_\delta, \\ c(\delta,t) = c_s(T(\delta,t)), \qquad t > t_\delta, \\ -G(\delta,t)\dot{\delta} + D\dfrac{\partial c}{\partial x}(\delta,t) = D_c(G,T)_{|(\delta,t)}\beta\dfrac{\partial T}{\partial x}(\delta,t), \qquad t > t_\delta, \\ \delta(t_\delta) = \xi(t_\delta). \end{cases} \tag{6.11}$$

The concentration profile $\bar{\bar{c}}(x)$ is the one at the exit from the previous stage. A glance at the free boundary condition $(6.11)_5$ reveals a quite serious mathematical difficulty in the study of this problem: at the transition time $t = t_\delta$ the coefficient of $\dot{\delta}$ vanishes. Condition $(6.11)_5$ is of Stefan type and the vanishing of the "latent heat" prevents the applicability of known theorems. Therefore a special analysis has to be devoted to the behaviour of the solution close to $t = t_\delta$. It has been proved that not only the solution exists, but also that $\dot{\delta}(t_\delta) = 0$, i.e. the desaturation front is in fact a C^1 continuation of the saturation front (though it can be shown that it cannot be C^2).

At some time t_γ the function $G(\eta^+, t)$ may reach the critical value G_{gel}. When this occurs the gelification front $x = \gamma(t)$, starting from $x = \eta(t_\gamma)$, appears. Such a front is defined by the implicit equation

$$G_{gel}(T(\gamma(t),t)) = -\mu\left[T(\gamma(t),t) - T(\gamma(t),\xi^{-1}(\gamma(t)))\right]. \tag{6.12}$$

For $x > \gamma(t)$ $G(x,t)$ is still defined through (6.9), while for $\eta(t) < x < \gamma(t)$ we have

$$\frac{\partial G}{\partial t} = \frac{\partial}{\partial x}\left(\beta D\frac{\partial T}{\partial x}\right) - \beta\frac{\partial T}{\partial t}, \tag{6.13}$$

where now D is not constant, but depends on G and T. From (6.13) we get

$$\begin{cases} \dfrac{\partial G}{\partial t} - \dfrac{\partial G}{\partial x}\left(\beta\dfrac{\partial D_c}{\partial G}\dfrac{\partial T}{\partial x}\right) = \beta\left(\dfrac{D_c}{D_T} - 1\right)\dfrac{\partial T}{\partial t} + \beta\dfrac{\partial D_c}{\partial T}\left(\dfrac{\partial T}{\partial x}\right)^2, \\ \\ G(\gamma,t) = G_{gel}(T(\gamma,t)) = -\mu\left[T(\gamma,t) - T(\gamma,\xi^{-1}(\gamma))\right], \end{cases} \tag{6.14}$$

which is the nonlinear first order PDE that governs the evolution of the solid phase concentration G. For $t > t_\gamma$ the deposit layer continues to grow according to (6.10) even though now $G(\eta^+, t)$ is evaluated through the solution of (6.14). It can be proved that G increases along the characteristics so that for some time t_ν it may reach the value G_{dep}. In addition it can be proved that the characteristic lines are intercepted by either $x = \nu(t)$, or $x = \delta(t)$ before any shock phenomenon takes place. This is of course crucial, since this possibility is indeed implicit in the mathematical structure of problem (6.14) (owing to the fact that the diffusivity of G has been neglected). The

assumptions made on the function $D(G,T)$ are essential in the demonstration of this important property.

At the time when $G = G_{dep}$ the diffusivity D vanishes and the deposit grows along the level set $x = \nu(t)$. If the front $x = \nu(t)$ does not appear, the front $x = \delta(t)$ can meet the deposit front while still decreasing. If, on the other hand, the front $x = \nu(t)$ does appear it can be proved that the depletion front has to invert its motion before meeting the deposit front. Stage 4 ends when the unsaturated region comes in touch with the deposit front and the system enters stage 5. During this stage the unsaturated region is governed by

$$\begin{cases} \dfrac{\partial c}{\partial t} = \dfrac{\partial}{\partial x}\left(D\dfrac{\partial c}{\partial x}\right), \quad \text{in } \ \theta(t) < x < L, \ \ t > t_\theta, \\ c(x,t_\theta) = \bar{\bar{c}}(x), \qquad \theta(t_\theta) < x < L, \\ \dfrac{\partial c}{\partial x}(L,t) = 0, \quad t > t_\theta, \\ c(\theta,t) = c_s(T(\theta,t)), \qquad t > t_\theta, \\ G_{dep}\dot{\theta} = D\dfrac{\partial c}{\partial x}(\theta,t), \qquad t > t_\theta \\ \theta(t_\theta) = \delta(t_\theta) = \nu(t_\theta), \end{cases} \tag{6.15}$$

where $x = \theta(t)$ represents the deposition front. The mathematical structure of problem (6.15) is again of the Stefan type. The final deposit thickness θ_∞ can be evaluated by the following mass balance

$$c^* L = \int_0^{\theta_\infty} G_\infty(x)dx + \int_0^{\theta_\infty} c_s(T_\infty(x))dx + c_s(T_\infty(\theta_\infty))(L - \theta_\infty). \tag{6.16}$$

where $c(\theta_\infty) = c_s(T(\theta_\infty))$ and where $G_\infty(x)$ is the asymptotic concentration of solid wax in the deposit. Condition for the existence and uniqueness of $\theta_\infty < L$ can be established. A marginal, but nontrivial, remark is concerned with the transition from stage 4 to stage 5. It may occur while $\dot{\delta}$ is negative, but there are cases in which the motion of the front $x = \delta(t)$ reverses its direction (becoming once more increasing) for a while before stage 5 is entered. This case is very technical and will not be discussed here.

7. Conclusions

We have reviewed a whole class of phenomena related with the process of the formation of wax deposit in non-isothermal WCO's. We have tried to highlight the complexity of the phase transition process and the phenomenon of thermally-induced wax migration in a saturated solution, which is the prevailing mechanism driving the formation of deposits in pipelines crossing cold regions. We have described the models allowing to interpret the data of the so-called cold finger device (both static and with agitation), so to obtain the values of wax diffusivity and solubility.

After that analysis we have sketched the deposition process in the pipelining of WCO's in non-isothermal conditions and in turbulent regime. Here we have taken into account various concurrent phenomena, such as ablation and ageing of the deposit, as well as the possible desaturation of the oil in a distant segment of the pipe.

Finally we have devoted a section to the study of a static WCO with a temperature evolution allowing the onset of gelification. The resulting problem is very complex, since various free boundaries can appear, separating regions evolving according to differential systems of different types. The mathematics becomes here particularly complicated, due to the occurrence of conditions which are non-standard in the free boundary problems of the classes considered. We believe that this is the first review paper in which all these subjects have been addressed and that it can be helpful for further investigations, which are indeed necessary since, for instance, a model for the WCO's pipelining including gelification is still missing.

Acknowledgements

Authors would like to thank eni exploration and production for technical and financial support of this work.

References

[1] M. Avrami. *Kinetics of Phase Change. I. General Theory*. J. Chem. Phys., 7 (1939), No. 12, 1103–1112.

[2] M. Avrami. *Kinetics of Phase Change. II. Transformation-Time Relations for Random Distribution of Nuclei*. J. Chem. Phys., 8 (1940), No. 2, 212–224.

[3] M. Avrami. *Kinetics of Phase Change. III. Granulation, Phase Change, and Microstructure*. J. Chem. Phys., 9 (1941), No. 2, 177–184.

[4] L.F.A. Azevedo, A.M Texeira. *A critical review of the modeling of wax deposition mechanisms*. Pet. Sci. Technol., 21 (2003), No. 3& 4, 393–408.

[5] E.D. Burger, T.K. Perkins, J.H.J Striegler. *Studies of wax deposition in the trans Alaska pipeline*. J. Pet. Technol., June (1981), 1075–1086..

[6] E. Comparini, F. Talamucci. *A general model for wax diffusion in crude oils under thermal gradient*, in Applied and Industrial Mathematics in Italy, (v. Cutello et al. eds.), World Scientific (2007), 259–270.

[7] S. Correra, A. Fasano, L. Fusi, M. Primicerio, F. Rosso. *Wax diffusivity under given thermal gradient: a mathematical model*, ZAMM Z.Angew. Math. Mech., 87 (2007), No. 1, 24–36.

[8] S. Correra, A. Fasano, L. Fusi, M. Primicerio. *Modelling of wax diffusion in crude oils: the cold finger device*, Appl. Math. Modl., 31 (2007), No. 10, 2286–2298.

[9] S. Correra, A. Fasano, L. Fusi L., D. Merino–Garcia D. *Calculating deposit formation in the pipelining of waxy crude oils*. Meccanica, 42 (2007), No. 2, 149–165.

[10] B. Coto, C. Martos, J.J. Espada, M.D. Robustillo, J.L. Peña. *Analysis of paraffin precipitation from petroleum mixtures by means of DSC: iterative procedure considering solid-liquid equilibrium equations*. Fuel, 89 (2010), 1087–1094.

[11] J.A.P. Coutinho, K. Knudsen, S.I. Andersen. *A local composition model for paraffinic solis solution*. Chem. Eng. Science, 51 (1996), No. 12, 3273–3282.

[12] J.A.P. Coutinho, V. Ruffier-Meary. *The use of differential scanning calorimetry in studies of wax deposition: measuring the solid formation and binary solid-liquid equilibrium phase diagrams*. Oil Gas Sci. Technol., 54 (1999), No. 5, 641–648.

[13] J.A.P. Coutinho, B. Edmonds, T. Moorwood, R. Szczepanski, X. Zhang. *Reliable wax predictions for flow assurance*. Energ. Fuel, 20 (2006) 1081–1088.

[14] J.C. Escobar-Remolina. *Prediction of characteristics of wax precipitation in synthetic mixtures and fluids of petroleum: a new model*. Fluid Phase Equilibr., 240 (2006) 197–203.

[15] L. Faienza. Mathematical models for wax deposition in crude oils. PhD Thesis, Dept. of Math., University of Florence (2010).

[16] A. Fasano, M Primicerio. *Heat and mass transfer in non-isothermal partially saturated solutions*. New Trends in Mathematical Physics,(P. Fergola et al. eds.), World Scientific (2003), 33–44.

[17] A. Fasano, M Primicerio. *Temperature driven mass transport in concentrated saturated solutions*. Prog. nonlin., 61 (2005), 91-108.

[18] A. Fasano, M Primicerio. *Wax deposition in crude oil: a new approach*. Rend. Mat. Acc. Lincei, 9 (2005), 251-263.

[19] A. Fasano, L. Fusi, J.R. Ockendon, M. Primicerio. *Gelification and mass transport in a static non-isothermal waxy solution*. Euro. J. of Appl. Math., 20 (2009), No. 1, 93–122.

[20] R. Gianni, A.G. Petrova. *One-dimensional problem for heat and mass transport in oil-wax solution*. Rend. Mat. Acc. Lincei, 9 (2005), 181–196.

[21] A.Hammami, A.K.Mehrotra. *Non-isothermal crystallization kinetics of n-paraffins with chain lenght between thirty and fifty*. Thermochim. Acta, 211 (1992), 137–153.

[22] A.Hammami, A.K.Mehrotra. *Non-isothermal crystallization kinetics of even-numbered and odd-numbered normal alkanes*. Thermochim. Acta, 215 (1993), 197–209.

[23] A.N. Kolmogorov. *In Russian*. Bull. Acad. Sci. USSR. Ser. Math., 3 (1937), 355–359.

[24] M. Margarone, R. Bagatin, C. Busto, P. D'Olimpio, L. Fusi, L. Faienza, A. Fasano, M. Primicerio. *A wax crystallization model from DSC experiments*. 11th International Conference on Petroleum Phase Behavior and Fouling, 13 - 17 June 2010, Jersey City, NJ, US.

[25] D. Merino-Garcia, M. Margarone, S. Correra. *Kinetics of waxy gel formation from batch experiments*. Energ. Fuel, 21 (2007), 1287–1295.

[26] T. Ozawa. *Kinetics of non-isothermal crystallization*. Polymer, 12 (1971), 150–158.

[27] S.K.Pedersen, P.Skovborg, P.D.Hans. *Wax Precipitation from North Sea Crude Oils: Thermodyamic Modeling*. Energ. Fuel, 5 (1991), 924–932.

[28] M. Primicerio. *Wax Segregation in Oils: A Multiscale Problem*. in Progress in Industrial Mathematics at ECMI 2008 (A.D.Fitt et al. eds.), Springer 2010, pp 43-68.

[29] E. Ramirez-Jaramillo, C. Lira-Galeana, O. Manero. *Modeling wax deposition in pipelines*. Petrol. Sci. Technol., 22 (2004), 821–861.

[30] P.Sajkiewicz, L.Carpaneto, A.Wasiak. *Application of the Ozawa model to non-isothermal crystallization of poly(ethylene terephthalete)*. Polymer, 42 (2001), 5365–5370.

[31] P. Singh, R. Venkatesan, H.S. Fogler, N. Nagarajan. *Formation and aging of incipient thin film wax-oil gels*. AIChE J., 46 (2000), No. 5, 1059–1074

[32] K.W.Won. *Thermodynamics for Solid Solution-Liquid-Vapor-Equilibria: Wax Phase Formation from Heavy Hydrocarbon Mixtures*. Fluid Phase Equilibr., 30 (1986), 265–279.

[33] Z.Zhang, C.Xiao, Z.Dong. *Comparison of the Ozawa and modified Avrami models of polymer crystallization under non-isothermal conditions using a commputer simulation method*. Thermochim. Acta, 466 (2007), 22–28.

[34] M.I.Zougari, T.Sopkow. *Introduction to Crude Oil Wax Crystallization Kinetics: Process Modeling*. Ind. Eng. Chem. Res., 46 (2007), 1360–1368.